INVERSE ANALYSIS OF HEAT TRANSFER IN FRICTION STIR WELDING USING GENERALIZED EXTREMAL OPTIMIZATION

Felipe Roman Centeno
Departamento de Engenharia Mecânica – Universidade Federal do Rio Grande do Sul – UFRGS – Porto Alegre, RS, Brazil
frcenteno@yahoo.com.br

Francis Henrique Ramos França
Departamento de Engenharia Mecânica – Universidade Federal do Rio Grande do Sul – UFRGS – Porto Alegre, RS, Brazil
frfranca@mecanica.ufrgs.br

Abstract. *Numerical simulations of a three-dimensional conduction heat transfer process are carried out to model the friction stir welding (FSW) of 304L Stainless Steel. A finite volume code was specifically developed by the authors to model friction stir welding, which is used together with an optimization code based on Generalized Extremal Optimization (GEO) method. The objective is to study the variation of transient temperature in a friction stir welded plate of 304L Stainless Steel. Based on the temperatures artificially measured at several locations on the plate for a given instant of time during the friction stir welding process, an inverse analysis of the thermal process is conducted using the GEO algorithm. The inverse analysis aims at determining the heat generated by friction between the tool shoulder and the workpiece as well as the unknown heat transfer coefficient between the workpiece and the supporting base, and between the air and the exposed surfaces of the plate. This paper demonstrates that the proposed inverse approach can be a very effective way to evaluate and predict in real time the parameters that govern the complex stir welding process, an important step towards its control.*

Keywords: *Friction stir welding, finite volume analysis, inverse analysis, numerical simulation, generalized extremal optimization.*

1. INTRODUCTION

Friction stir welding (FSW) is a relatively new, state-of-the-art solid state joining process. This metal joining technique is derived from the conventional friction welding. In a typical FSW, a rotating cylindrical pin tool is forced to plunge into the plates to be welded (i.e. workpiece) and moved along their contact line. During this operation, frictional heat that is generated by contact friction between the tool and workpiece softens the material. The plasticized material is stirred by the tool and forced to "flow" to the side and the back of the tool as the tool advances. As the temperature cools down, a solid continuous joint between the two plates is then formed. Because the highest temperature in the FSW process is lower than the melting temperature of the workpiece material, FSW yields fine microstructures, absence of cracking, low residual distortion and no loss of alloying elements that are the main advantages of this solid phase process. Nevertheless, as in the traditional fusion welds, a softened heat affected zone and a tensile residual stress parallel to the weld also exist.

Although it is a new welding technology, the FSW has been extensively studied in both the academic and industrial communities for most aluminum alloys including difficult-to-weld alloys such as AA2195 (with lithium) and AA7075. Most of the researchers have focused their attentions on the heat transfer or temperature analysis of FSW. Tang et al. (1998) presented the experimentally measured temperature distributions of the workpiece in an FSW. Gould and Feng (1998) proposed a simple heat transfer model for predicting the temperature distribution in the workpiece of the FSW. Chao and Qi (1998, 1999) developed a moving heat source model in a finite element analysis and simulated the transient temperature, residual stress and residual distortion of the FSW process. Furthermore, Colegrove et al. (2000) and Frigaard et al. (2001) developed three-dimensional heat flow models for the prediction of temperature fields in the FSW. Midling (1999), Russell and Sheercliff (1999) investigated the effect of tool shoulder material and pin tool on heat input during the FSW. More recently, Donne et al. (2001) reported the measured residual stresses in friction stir welds for 2024-T3 and 6013-T6 aluminums. Dong et al. (2001) carried out a coupled thermo-mechanical analysis of the FSW process using a simplified two-dimensional axisymmetric model. Chao et al. (2003) investigated the variations of heat energy and temperature produced by the FSW in both the workpiece and the pin tool. All investigations show that the FSW process of aluminum alloys yield welds with low distortion, high quality and low cost. Consequently, better structural performance is the primary advantage of this technology. For example, a demonstration of the tremendous potential and successful applications of aluminum FSW in airframe structures can be found in Talwar et al. (2000).

In principle, the FSW process can be applied to joining other alloy materials such as steels and titanium as well. Of course, it is well known that current tool materials used in the FSW for aluminums are not adequate for production applications in many of the harder alloy materials. However, when adequate wear resistant tool materials become available, the benefits of the FSW may promote its rapid implementation in the production of ferrous structures and structures made from other more refractory materials. While the development of tool materials is still an ongoing

research field, it is also important to make progress in the development of the FSW process for steels. For instance, experimental studies of austenitic stainless steels (Reynolds et al., 2000) revealed the microstructures, residual stresses and strength of the friction stir welds. To further understand the fundamental mechanisms associated with the welding formation process and improve the welding quality for the FSW of steels, numerical modeling and simulations of transient temperature and residual stresses are valuable and necessarily needed.

Recently Zhu and Chao (2004) conducted a three-dimensional nonlinear thermal and thermo-mechanical numerical simulations for the FSW of 304L stainless steel. The study considered the variation of transient temperature and residual stress in a friction stir welding of a 304L stainless steel plate by using a finite element analysis. Based on the experimental measurements of the transient temperatures at several locations on the plate, an inverse analysis method for thermal numerical simulation was carried out to estimate some of the thermal parameters that govern the welding process.

The present paper considers the solution of the transient three-dimensional heat conduction equation for the friction stir welding of 304L stainless steel using the finite volume analysis. Based on artificial measurements of temperature at different locations on the plate, an inverse analysis is carried out based on the optimization of an objective function. This function is defined as the error between the measured temperatures and the temperatures determined from the estimated parameters, which are: the heat input by the tool into the workpiece, the heat transfer coefficient between the workpiece and the support base, and the heat transfer coefficient between the workpiece and the surroundings (i.e., the ambient). The optimization problem is solved with the Generalized Extremal Optimization (GEO) algorithm (Sousa et al., 2003). Measurement data for the temperatures are fabricated from exact values of temperatures obtained from a numerical solution performed by a given set of parameters, which are then perturbed with noises related to a set of standard deviations.

2. PROBLEM DEFINITION

The modeled process considers the welding of two thin plates of 304L stainless steel using the friction stir welding (FSW) process. Each plate has 304.8 mm in length, 101.6 mm in width and 3.18 mm in thickness. The pin tool has a shoulder diameter of 19.05 mm, and a pin diameter of 6.35 mm. The geometry of the workpiece and the pin tool in a typical FSW is shown in Fig. 1. The pin tool starts at 6.4 mm away from the edge, and stops after translation of 279.4 mm along the weld line. The tool rotational speed is 300 rpm, and the tool translation velocity is of 1.693 mm/s; in this manner, the total welding time is 165 s. There is a pre-heat time of 6 seconds, in which the tool stands still at a distance of 6.4 mm from the border before it begins the translation.

An artificial experiment is executed in order to obtain temperatures at ten specific points shown in Fig. 2, which are used as the input information for the inverse analysis. These ten points are located at the top and at the bottom surfaces of the plate (5 in each surface), exactly in the middle of it in the *x*-direction, and at 11.36, 15.00, 21.79, 28.42 and 38.21 mm from the welding line in the *y*-direction. These ten temperatures are measured at the moment the tool is passing through the middle *x*-position of the plate.

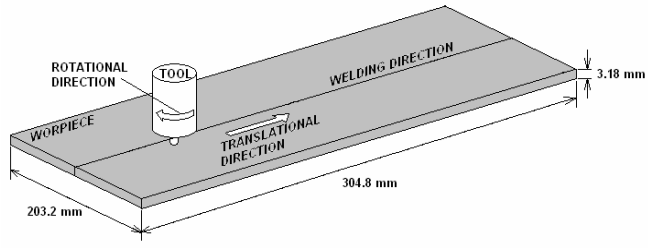

Figure 1. Geometry configuration of *FSW*

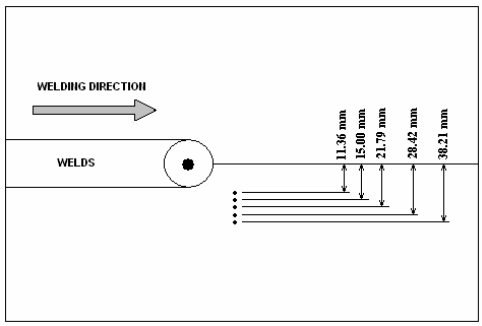

Figure 2. Locations of the temperature measurement

3. NUMERICAL ANALYSIS

3.1. Finite volume method for transient heat transfer modeling

The transient temperature distribution T on the plate depends on the time t and the spatial coordinates (x, y, z), and is determined by the solution of the three-dimensional diffusion equation:

$$\rho c \frac{\partial T}{\partial t} = \frac{\partial}{\partial x}\left(k\frac{\partial T}{\partial x}\right) + \frac{\partial}{\partial y}\left(k\frac{\partial T}{\partial y}\right) + \frac{\partial}{\partial x}\left(k\frac{\partial T}{\partial y}\right) \tag{1}$$

where k is the coefficient of thermal condutivity, W/(m.K), c is the specific heat capacity, J/(kg.K), and ρ is the density of the material, kg/m³. The friction stir welding is treated as a heat source moving along the line of the welding line. The heat produced by the friction between the pin tool shoulder and the plate is concentrated locally, and propagates into the other regions of the plates by conduction, in addition to the losses by convection and radiation on the boundaries. It is assumed that the heat flux S (in W/m²) is uniformly distributed at the pin tool shoulder, so the heat input Q (in W) can be computed by the product between S and the shoulder area. The heat generated at the pin of the tool is neglected because it is comparatively very small, e. g. in the order 2% of the total heat (Russell and Sheercliff, 1999). As such, only the heat flux imposed by the tool shoulder is considered. The heat input Q (or, alternatively, S) is unknown, its determination being one of the objectives of the present inverse.

On the boundaries (surfaces) of the workpiece, convection and radiation heat transfer are responsible for heat loss to the ambient, which are given by:

$$q''_{conv} = h_{conv}\left(T - T_{\infty}\right) \tag{2a}$$

$$q''_{rad} = \varepsilon\sigma\left(T^4 - T_{sur}^4\right) \tag{2b}$$

The total heat loss, in W/m^2, is given by:

$$q'' = q''_{conv} + q''_{rad} \tag{3}$$

where T_{∞} is the environment temperature, in K, h_{conv} is the convection coefficient, in W/(m²·K), T_{sur} is the surroundings temperature, in K, ε is the emissivity of the plate surfaces, assumed as gray emitters, and σ if the Stefan-Boltzman constant, 5.67x10^{-8} W/(m²·K). In this calculation, T_{∞} = 303 K, T_{sur} = 303 K, h_{conv}= 10 W/(m²·K) and ε = 0.17 are set to describe the process. Actually, the value of h_{conv} will be treated as an unknown and will be also determined by the inverse analysis. The heat loss from the bottom surface is due to heat conduction from the workpiece and support base plate, which depends on the geometry of the base as well as of the contact thermal resistance. An accurate evaluation of this heat loss is not a simple task, but experience has shown that it can be described by a rather simple relation that is similar to that used for the convection heat transfer, that is:

$$q''_b = h_b\left(T - T_b\right) \tag{4}$$

where h_b is the heat transfer coefficient, in W/(m²·K), between the plate and the base, and T_b is the non-perturbed temperature of the base (that is, not affected by the contact with the plate), assumed here to be at the same value of the environment and surroundings, T_b = 303 K. The simple relation for the heat loss to the base requires the knowledge of the heat transfer coefficient between the plate and the supporting base, h_b. The objective of the inverse analysis is to determine h_b, in addition to the heat input Q and the convective coefficient h_{conv}, from measurements of the temperature.

Furthermore, in the numerical simulation of the FSW for 304L stainless steel, it is assumed that the two plates are welded symmetrically during and after the welding. The welding line is along the symmetry line, and thus only one-half of the welded plate is modeled. The Finite Volume Method (FVM) mesh is shown in Fig. 3, which has 122, 13 and 5 volumes in the x, y and z directions. The mesh is non-uniform in the y-direction: it has 8 volumes in the first 20 mm in the y-direction, and the remaining width of the plate is divided into 5 volumes, which obey a tangent-hiperbolic refinement equation.

Figure 4 shows the temperature distribution along the transverse direction at x =152.4 mm (at time of 86 s) for different refinement meshes. It can be observed that in a mesh sensitivity study of welding simulation, using meshes more refined than the one used in the current work (a total of 7930 volumes) generated nearly identical results, but the computational time increased significantly. A time step of 1.0 second was used for all simulations.

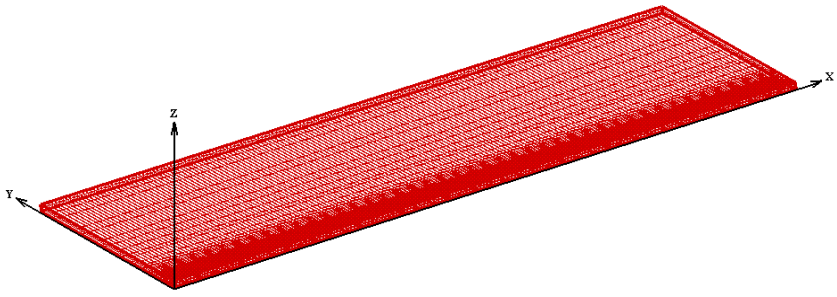

Figure 3. Finite volume method mesh.

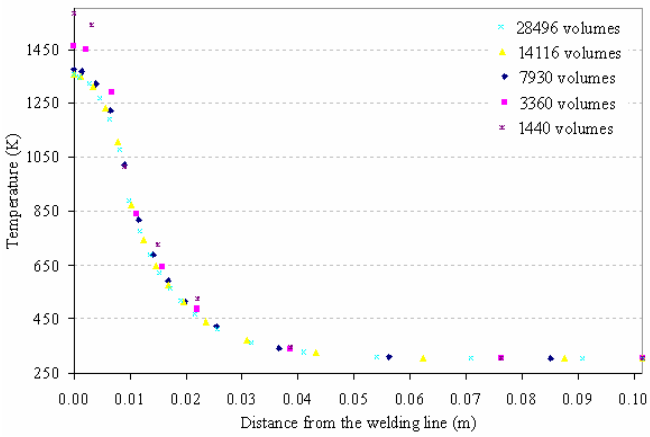

Figure 4. Mesh sensitivity study.

The material properties of 304L stainless used in the FVA computation are taken from the Metals Handbook of Brown et al. (1993). The thermal properties are determined by the following relations (temperature T in ^{o}C):

$$k(T \le 1000\,°C) = 7.254902 + 0.04155462\,2T - 0.00002065\,8263T^2 \quad \text{[W/m·K]} \tag{5a}$$

$$k(T > 1000\,°C) = 0.0004232T \quad \text{[W/m·K]} \tag{5b}$$

$$\rho = 8021.4286 - 1.3035714T + 0.00044542857T^2 \quad \text{[kg/m}^3\text{]} \tag{5c}$$

$$c = \frac{580}{\left(1 + \exp\left(273.92495 - 0{,}42631809T\right)\right)^{11399.278}} \quad \text{[J/kg·K]} \tag{5d}$$

3.2. Generalized extremal optimization (GEO) method

The generalized extremal optimization (GEO) algorithm (Sousa et al., 2003) is a new evolutionary algorithm devised to improve the Extremal Optimization method (Boettcher and Percus, 2001) so that it could be easily applicable to virtually any kind of optimization problem. Both algorithms were inspired by the evolutionary model of Bak and Sneppen (1993). Following the Bak and Sneppen (1993) model, in GEO L species are aligned and for each species it is assigned a fitness value that will determine the species that are more prone to mutate. One can think of these species as bits that can assume the values of 0 or 1. Hence, the entire population would consist of a single binary string. The design variables of the optimization problem are encoded in this string that is similar to a chromosome in a genetic algorithm (GA) with binary representation (see Fig. 5).

To each species (bit) it is assigned a fitness number that is proportional to the gain (or loss) the objective function value has in mutating (flipping) the bit. All bits are then ranked from rank 1, for the least adapted bit, to N for the best adapted. A bit is then mutated (flipped) according to the probability distribution (1). This process is repeated until a given stopping criteria is reached and the best configuration of bits (the one that gives the best value for the objective function) found through the process is returned.

The practical implementation of the canonical GEO algorithm to a function optimization problem is as follow:

1. Initialize randomly a binary string of length L that encodes N design variables of bit length l_j (j = 1, N). For the initial configuration C of bits, calculate the objective function value V and set $C_{best} = C$ and $V_{best} = V$.
2. For each bit i of the string, at a given iteration:
   a) flip the bit (from 0 to 1 or 1 to 0) and calculate the objective function value V_i of the string configuration C_i;
   b) set the bit fitness as $\Delta V_i = (V_i - V_{best})$. It indicates the relative gain (or loss) that one has in mutating the bit, compared to the best objective function value found so far;
   c) return the bit to its original value.
3. Rank the bits according to their fitness values, from k = 1 for the least adapted bit to $k = L$ for the best adapted. In a minimization problem, higher values of ΔV_i will have higher ranking, and otherwise for maximization problems. If two or more bits have the same fitness, rank them randomly with uniform distribution.
4. Choose with uniform probability a candidate bit i to mutate (flip from 0 to 1 or from 1 to 0). Generate a random number RAN with uniform distribution in the range [0,1]. If $P_i(k) = k^{-\tau}$ is equal or greater than

RAN the bit is confirmed to mutate. Otherwise, choose a new candidate bit and repeat the process until a bit is confirmed to mutate.

5. Set $C = C_i$ and $V = V_i$, with i the bit confirmed to mutate in step 4.
6. Repeat steps 2 to 6 until a given stopping criteria is reached.
7. Return C_{best} and V_{best} *found during the search*.

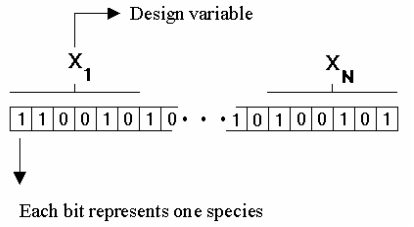

Figure 5. Design variables encoded in a binary string.

Note that in step 4 any bit can be chosen to mutate, but the probability of a given chosen bit be confirmed to mutate is dependent on its rank position. The ones more adapted (with higher rank values) are less prone to have its mutation confirmed and only the least adapted bit (rank = 1) is always confirmed to mutate, if chosen. The probability of mutating the chosen bit is regulated by the adjustable parameter τ. The higher the value of τ, the smaller the chance of a bit (with rank greater than 1) be mutated. The possibility of making moves that do not improve the value of the objective function is what allows the algorithm to escape from local optima.

In a practical application of the GEO algorithm, the first decision to be made is on the definition of the number of bits that will represent each design variable. This can be done simply setting for each variable the number of bits necessary to assure a given desirable precision for each of them. For continuous variables the minimum number (m) of bits necessary to achieve a certain precision is given by:

$$2^m \geq \left[\frac{\left(x_j^u - x_j^l \right)}{p} + 1 \right] \tag{6}$$

where x_j^l and x_j^u are the lower and upper bounds, respectively, of the variable j (with j = 1, N), and p is the desired precision. The physical value of each design variable is obtained through the equation:

$$x_j = x_j^l + \left(x_j^u - x_j^l \right) \frac{I_j}{\left(2^m - 1 \right)} \tag{7}$$

where I_j is the integer number obtained in the transformation of the variable j from its binary form to a decimal representation.

3.2.1. Taking into account discrete and integer variables

As we have seen above, continuous variables are represented in the GEO in binary form, with precision p. Integer variables have precision p = 1 and may be treated such as presented in Lin and Hajela (1992) for a binary coded GA. If the relation $\left(x_j^u - x_j^l \right) = 2^N - 1$ is satisfied, there is a string of bits that will encode all variables biunivocaly. If there is not a direct correspondence between one sequence of bits and the variables, the smallest number m that satisfies $2^m > \left(x_j^u - x_j^l \right) + 1$ is calculated and for each of the N variables it is associated one sequence of bits. To the remaining $2^m - N$ strings, integers out of the range of the variables are attributed, which are treated as unfeasible solutions. (How GEO deals with constraints is described in the next sub-section). Integers within the feasible interval may also be used. In this case, one or more variables will be associated with more than one sequence of bits. Although this last option avoids the necessity of imposing additional constraints to the problem, it implies, in the case of the GEO, a non-uniform probability for the selection process of the bit to be mutated in step 4.

Discrete variables may be treated in the same way as the integer variables. The process is carried out in two steps: first, to each discrete variable an integer number is associated and, second, one of the approaches described before is used to code them into binary form.

3.2.2. How GEO deals with constraints

Constraints in design optimization can be handled by many different ways. A simple, and probably the most common, way to deal with constraints in algorithms such as the GA and the simulated annealing (SA) is to incorporate them into the objective function via penalties. In evolutionary algorithms the penalty function approach have been extensively used in different types of implementations. Methods that deal directly with the constraints have been also proposed in order to avoid the process of setting the penalty parameters, since their values are highly problem dependent and if not properly set can lead to sub-optimal designs. Alternatively, adaptive penalty schemes have been proposed in such a way that the parameters are set automatically, without the need of fine tuning them for a particular application.

For GEO, side constraints (the bounds on the design variables) are directly incorporated when the design variables are encoded in binary form. Equality and inequality constraints are easily incorporated into the algorithms simply setting a high (for a minimization problem) or low (for a maximization problem) fitness value to the bit that, when flipped, leads the configuration to an unfeasible region of the design space. For example, in a minimization problem, when the fitness values are attributed to the bits in step 2, the ones that when flipped result in a non-feasible configuration receive a high value for ΔV_i (the same value is attributed to all bits in which this occurs). This means that those bits will be considered well adapted and will have a low probability to be flipped in step 4. However, they are not forbidden to be flipped, what makes the algorithm able to walk through infeasible regions of the design space. This gives a great flexibility to the algorithm that can, for example, be applied to design spaces that present disconnected feasible regions. In fact, the GEO can even start from an infeasible solution. In this case a dummy value is attributed to V_{best} in the initialization of the algorithm, which is replaced by the first feasible value of V found during the search.

It must be pointed out here, that other ways to take into account constraints in GEO may also be easily implemented, including the penalty function approach. However, the approach described above is very simple to apply and does not introduce any new adjustable parameter in the algorithm.

4. SOLUTION METHODOLOGY

A simple, effective way of testing the proposed inverse analysis is to simulate the FSW process and, for given values of Q, h_b and h_{conv}, obtain the temperatures at the measurement locations shown in Fig. 2. Then, the inverse analysis is carried out to verify if the values of Q and h_b (for study case 1) and Q, h_b and h_{conv} (for study case 2) can be correctly recovered. To consider a more realistic situation, when the temperature measurements are affected by errors, the values of the temperatures obtained from the numerical simulations (for given values of Q, h_b and h_{conv}) will be perturbed by a noise according to a prescribed standard deviation u (the most common symbol, σ, will be avoided here not to confuse with the Stefan-Boltzmann constant). The objective is to evaluate how these noises can affect the estimation of Q and h_b (for study case 1) and of Q, h_b and h_{conv} (for study case 2). The procedure of disturbing the numerical values of the temperatures will be denominated numerical-experimental values.

The procedure of the numerical-experiment method is outlined as follows:

1. Specify a value for the natural convection coefficient, h_{conv} in Eq. (2a). A reasonable guess is h_{conv} = 10 W/m²K;
2. Specify a value for the fictitious convection coefficient, h_b in Eq. (4). It will be taken as 10 times the typical natural convection coefficient. Thus, h_b = 100 W/m²K;
3. Specify a value for the total heat input energy, Q, produced by the contact friction between the tool shoulder and the plates. As will be verified, a reasonable guess is Q = 760 W;
4. Solve the three-dimensional differential equation (1), under the boundary conditions of (2)–(4), using the finite volume numerical method. The solution of the resulting system of equations were accomplished with the TDMA method, setting a maximum relative temperature error between two subsequent iterations as 10^{-6};
5. Determine and store the temperature values at the ten locations shown in Fig. 2 for a given instant of time (which is 92 seconds);
6. Generate 10 random numbers ($rand_i$) between 0 and 1;
7. Compute: $\zeta_i = 0.5\text{-}rand_i$. With the value of ζ_i select the value of η_i from a table of integrals of the gaussian normal error function;
8. Choose the value of the standard deviation (u): 0, 0.25, and 0.5 K.
9. Compute the value of the numerical-experimental temperatures: $T_i^{'} = T_i + \eta_i u$.

Steps 6 to 9 simulate measurement errors following a Gaussian distribution function with standard deviation of u.

Once the experimental temperatures are provided, the thermal-optimization analysis can be executed following the steps below (the values of the parameters used in this work are described together with the steps):

1. Specify the range of the parameters which will be optimized:
    a. Total heat generated by friction: 200 W $\leq Q \leq$ 2000 W;

b. Heat transfer coefficient at the bottom surface: 20 W/m²K $\leq h_b \leq$ 200 W/m²K;
c. Convective heat transfer coefficient (used only in case 2): 1 W/m²K $\leq h_{conv} \leq$ 100 W/m²K;

2. Specify the number of function evaluations (*NFE*) at each τ: *NFE = 1000*, for 1.25 ≤ τ ≤ 2.0 (τ is changed in steps of 0.25);
3. Specify the objective function as $F(Q,h_b)=\sum_{i=1}^{I}\left[(T_i^{'}-T_{i,cal})^2\right]^{1/2}$, where $T_{i,cal}$ is the temperature computed in point *i* for given values of *Q* and h_b, and *I* is equal to number of measurement points, *I* = 10;
4. Run GEO and obtain the value of τ_{best} that return the minimum value of $F(Q,h_b)$ (this should provide the best estimates for *Q* and h_b);
5. Set τ =τ_{best} (it was found that τ_{best} = 1.25) and enlarge *NFE (NFE* = 10000*)* for greater refinement;
6. Run GEO and obtain the final values for *Q* and h_b.

It should be noted that the number of function evaluations (*NFE*) is equal to the number of times that the finite volum code is run for each τ, which means that the finite volume code must be as quick as possible in order to accelerate the optimization process, which is time consuming due to its evolutionary nature.

5. NUMERICAL-EXPERIMENTAL RESULTS

Using the numerical-experimental method discussed in Section 4, heat transfer simulations are performed for FSW of 304L stainless steel. The variation of temperature obtained from this analysis along the transverse direction at the middle *x*-direction is shown in Fig. 6. As it is expected physically, the difference between the temperatures at the bottom and at the top surfaces are very small, since the material is highly conductive and the plate is thin. Moreover, the temperatures fall rapidly to the environmental temperature for positions far from the welding line. Figure 7 illustrates the temperature contour at welding time 111 s. It is seen that the highest temperature during welding is within the tool shoulder and has the value of 1430 K, which is less than the melting temperature 1723 K of 304L stainless steel. In fact, the 304L steel is not expected to melt during the FSW, since it is generally accepted that this is a solid-state jointing process. The value that was set for the heat input, *Q* = 760 W, can therefore be considered reasonable.

The temperatures shown in Figs. 6 and 7 can be considered "exact" in the sense that they are not affected by measurements errors. For a realistic real-time estimation of parameters *Q* and h_b, the temperatures should be perturbed by a noise according to the standard deviation of the measurement procedure. This is accomplished following the procedure outlined in Section 4. In Table 1, it is presented, for each measurement point in the *y*-position on the top and on bottom positions, the values of η that give a measure of how distant the measured temperature is from the mean Gaussian temperature (which can be understood as the exact value). Random numbers between 0 and 1 are generated so that the temperature noises follow a Gaussian curve. Finally, in Table 2, it is shown the numerical-experimental temperatures for noises with standard deviation *u* of 0, 0.25 and 0.5 K.

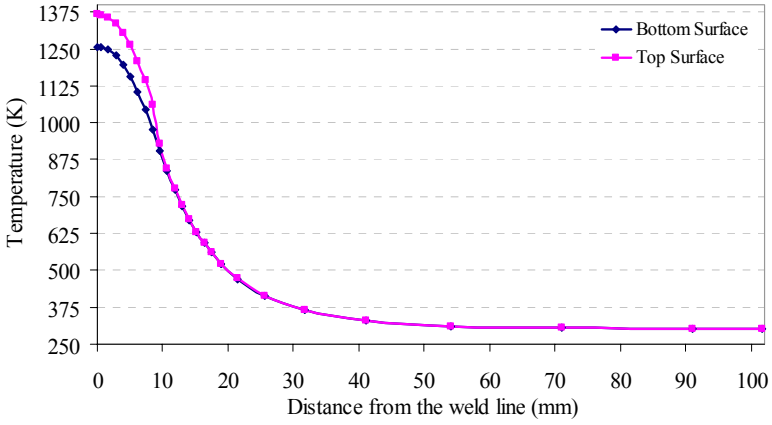

Figure 6. Distribution of temperature along the transverse direction for *x* =152.4 mm (at time of 86 s).

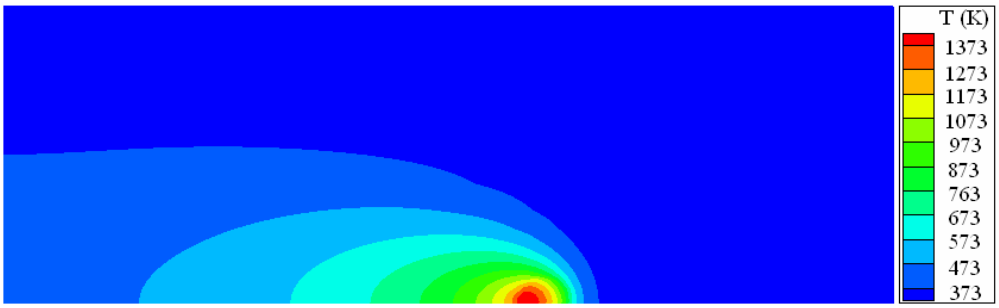

Figure 7. Simulated temperature contour at welding time 111 s (top surface of the plate).

Table 1. Gaussian normal error function.

	Top Surface					Bottom Surface				
y distance (mm)	11.36	15.00	21.79	28.42	38.21	11.36	15.00	21.79	28.42	38.21
Rand	0.268	0.095	0.640	0.917	0.809	0.725	0.111	0.096	0.622	0.538
ζ	0.232	0.405	-0.140	-0.417	-0.309	-0.225	0.389	0.404	-0.122	-0.038
η	0.620	1.310	-0.360	-1.390	-0.880	-0.600	1.220	1.300	-0.310	-0.100

Table 2. Numerical-experimental temperatures, $T_i^{'}$ (K).

y location (mm)	Top Surface			Bottom Surface		
	u =0.0 K	*u* =0.25 K	*u* =0.50 K	*u* =0.0 K	*u* =0.25 K	*u* =0.50 K
11.36	869.565	869.72	869.875	869.005	868.855	868.705
15.00	625.428	625.7555	626.083	625.314	625.619	625.924
21.79	471.394	471.304	471.214	471.129	471.454	471.779
28.42	382.618	382.2705	381.923	382.429	382.3515	382.274
38.21	357.568	357.348	357.128	357.346	357.321	357.296

6. RESULTS

After some runs of the GEO algorithm, it was found that the optimum value for τ was τ_{best} = 1.25 for case 1 and was τ_{best} = 0.25 for case 2. For these τ, a total of 10,000 evaluations of the objective functions were executed in order to find the best solutions for each case. Tables 3, 4 and 5 present the estimates of Q and h_b and tables 6, 7 and 8 present the estimates of Q, h_b and h_{conv} obtained from the numerical-experimental temperatures for standard deviation of u = 0.0 K, u = 0.25 K and u = 0.50 K. The best values found by GEO in case 1 for Q and h_b are shown in Table 3, which also presents the percentage errors with respect to the target values of these parameters and the objective function values for each u ~~case~~. Similarly, the best values found by GEO in case 2 for Q, h_b and h_{conv} are shown in Table 6, which also presents the percentage errors with respect to the target values of these parameters and the objective function values for each u. These errors indicate that the heat rate generated by friction, Q, has a stronger effect on the plate measured temperatures in comparison to the heat transfer coefficient at the bottom surface, h_b, and the natural convective coefficient, h_{conv}, since the errors for Q are smaller than those for h_b and h_{conv}. A comparison between the objective temperatures (which include the experimental noise) and the calculated temperatures for the selected values of Q and h_b (GEO algorithm) are presented in Tables 4 and 5 for the top and bottom surfaces, respectively, for case 1, and in Tables 7 and 8 for the top and bottom surfaces, respectively, for case 2. These comparisons in general show a satisfactory agreement.

Table 3. GEO results for case 1: frictional heat input (Q), heat transfer coefficient at bottom surface (h_b) and objective function value.

u (K)	*Q* (W)	Relative Error (on *Q*)	h_b (W/m²·K)	Relative Error (on h_b)	Objective function value (K)
0.00	379.438	0.148 %	97.479	2.521 %	0.861
0.25	381.048	0.276 %	105.006	5.006 %	1.089
0.50	380.937	0.246 %	105.006	5.006 %	1.698
Target	380.000	-	100.000	-	0.00

Table 4. Comparison between the target ($T_i^{'}$) and the calculated ($T_{i,cal}$) temperatures for the top surface (case 1).

y location (mm)	*u* = 0.0 K		*u* = 0.25 K		*u* = 0.50 K	
	$T_i^{'}$ (K)	$T_{i,cal}$ (K)	$T_i^{'}$ (K)	$T_{i,cal}$ (K)	$T_i^{'}$ (K)	$T_{i,cal}$ (K)
11.36	869.565	869.895	869.720	869.419	869.875	870.053
15.00	625.428	625.564	625.755	625.968	626.083	626.881
21.79	471.394	471.121	471.304	471.83	471.214	471.776
28.42	382.618	382.307	382.270	382.578	381.923	381.950
38.21	357.568	357.419	357.348	357.431	357.128	357.004

Table 5. Comparison between the target ($T_i^{'}$) and the calculated ($T_{i,cal}$) temperatures for the bottom surface (case 1).

y location (mm)	*u* = 0.0 K		*u* = 0.25 K		*u* = 0.50 K	
	$T_i^{'}$ (K)	$T_{i,cal}$ (K)	$T_i^{'}$ (K)	$T_{i,cal}$ (K)	$T_i^{'}$ (K)	$T_{i,cal}$ (K)
11.36	869.005	869.093	868.855	868.713	868.705	868.709
15.00	625.314	625.240	625.619	626.210	625.924	627.051
21.79	471.129	470.814	471.454	472.479	471.779	473.255
28.42	382.429	382.097	382.351	382.972	382.274	382.884
38.21	357.346	357.192	357.321	357.606	357.296	357.569

Table 6. GEO results for case 2: frictional heat input (Q), heat transfer coefficient at bottom surface (h_b) and natural convective coefficient (h_{conv}) and objective function value.

u (K)	*Q* (W)	Relative Error (on *Q*)	h_b (W/m²·K)	Relative Error (on h_b)	h_{conv} (W/m²·K)	Relative Error (on h_{conv})	Objective function value (K)
0.00	379.768	0.061 %	98.597	1.403 %	10.172	1.720 %	0.719
0.25	379.768	0.061 %	98.597	1.403 %	10.172	1.720 %	2.259
0.50	381.318	0.346 %	107.679	7.679 %	6.472	35.28 %	4.072
Target	380.000	-	100.000	-	10.000	-	0.00

Table 7. Comparison between the target ($T_i^{'}$) and the calculated ($T_{i,cal}$) temperatures for the top surface (case 2).

y location (mm)	*u* = 0.0 K		*u* = 0.25 K		*u* = 0.50 K	
	$T_i^{'}$ (K)	$T_{i,cal}$ (K)	$T_i^{'}$ (K)	$T_{i,cal}$ (K)	$T_i^{'}$ (K)	$T_{i,cal}$ (K)
11.36	869.565	869.635	869.72	869.945	869.875	869.125
15.00	625.428	625.391	625.7555	626.0465	626.083	626.235
21.79	471.394	471.294	471.304	471.114	471.214	470.967
28.42	382.618	382.523	382.2705	381.8285	381.923	290.308
38.21	357.568	357.543	357.348	357.103	357.128	356.731

Table 8. Comparison between the target ($T_i^{'}$) and the calculated ($T_{i,cal}$) temperatures for the bottom surface (case 2).

y location (mm)	*u* = 0.0 K		*u* = 0.25 K		*u* = 0.50 K	
	$T_i^{'}$ (K)	$T_{i,cal}$ (K)	$T_i^{'}$ (K)	$T_{i,cal}$ (K)	$T_i^{'}$ (K)	$T_{i,cal}$ (K)
11.36	869.005	868.963	868.855	868.363	868.705	867.979
15.00	625.314	625.227	625.619	625.837	625.924	626.341
21.79	471.129	471.003	471.454	471.652	471.779	472.528
28.42	382.429	382.321	382.351	382.165	382.274	382.287
38.21	357.346	357.319	357.321	357.270	357.296	357.302

7. CONCLUSIONS

This paper considered the estimation of parameters for the friction stir welding (FSW) of a 304L Stainless Steel plate. The estimation was carried out by means of an optimization problem, in which the objective function corresponded to an error fucntion between the measured temperature and the temperature computed for each estimated value of the heat rate input and the heat transfer coefficient on the bottom of the plate. The time-dependent temperature distribution on the plate was determined by the solution of the three-dimensional transient state diffusion equation, which was solved by the control-volume method. The minimization of the objective function was accomplished with the aid of the Generalized Extremal Optimization (GEO) algorithm, an evolutionary method that can deal with virtually

any type of optimization problem. The estimation of the heat rate input in the tool shoulder, the heat transfer coefficient on the bottom of the plate, and the natural convective coefficient was carried out from the measurement of ten temperatures located on the top and bottom surfaces of the plate. To simulate real-data measurements, the temperature inputs, obtained from a numerical solution for specific values of the heat input and the heat transfer coefficient, were perturbed with noises according to the standard deviation of the measurement procedure. Overall, the proposed methodology was capable of providing a satisfactory estimate for the three unknown parameters. For the heat input rate, the error was less than 1.0%, while for the heat transfer coefficients it reached 35%. The small error in the estimate of the heat input rate indicates that its effect on the temperature distribution on the plate is more important than the effect of the heat transfer coefficients. As a next step in the research, the modeling of the heat generated in the tool shoulder can be sophisticated, treating it as a non-uniform heat flux in the region around the tool shoulder. This will lead to more parameters to be estimated, which in turn will impose a more difficult problem to be solved.

8. ACKNOWLEDGEMENTS

The first author thanks CNPq due to its financial support by means of a Masters Degree scholarship to the first author. We also thank Dr. Fabiano Luis de Sousa (INPE) for providing the GEO algorithm code.

9. REFERENCES

Bak, P. and Sneppen, K., 1993, "Punctuated Equilibrium and Criticality in a Simple Model of Evolution", Physical Review Letters, Vol. 71, Number 24, pp. 4083-4086.

Boettcher, S. and Percus, A.G., 2001, "Optimization with Extremal Dynamics*",* Physical Review Letters, Vol. 86, pp. 5211-5214.

Brown W.F., Mindlin H., and Ho C.Y.,1993, Aerospace Structural Metals Handbook, CINDAS/USAF CRDA Handbooks Operation and Purdue University, West Lafayette, IN, USA.

Chao Y.J., and Qi X., 1998, "Thermal and thermo-mechanical modeling of friction stir welding of aluminum alloy 6061-T6", J. Mater. Process. Manuf. Sci. 7, pp. 215-233.

Chao X.J., and Qi X., 1999, "Heat transfer and thermo-mechanical modeling of friction stir joining of AA6061-T6 plates", Proceedings of the First International Symposium on Friction Stir Welding, Thousand Oaks, CA, USA..

Chao Y.J., Qi X., and Tang W., 2003, "Heat transfer in friction stir welding - experimental and numerical studies", ASME J. Manuf. Sci. Eng. 125, pp. 138-145.

Colegrove P., Pinter M., Graham D., and Miller T., 2000, "Three dimensional flow and thermal modeling of the friction stir welding process", Proceedings of the Second International Symposium on Friction Stir Welding, Gothenburg, Sweden, pp. 26-28.

Dong P., Lu F., Hong J.K., and Cao Z., 2001, "Coupled thermomechanical analysis of friction stir welding process using simplified models", Sci. Technol. Weld. Jointing 6, pp. 281-287.

Donne C.D., Lima E., Wegener J., Pyzalla A., and Buslaps T., 2001, "Investigations on residual stresses in friction stir welds", Proceedings ofthe Third International Symposium on Friction Stir Welding, Kobe, Japan, pp. 27–28.

Frigaard O.,Grong O., and Midling O. T., 2001, "A process model for friction stir welding of age hardening aluminum alloys", Metal. Mater. Transition A 32, pp. 1189-1200.

Gould J., and Feng Z., 1998, "Heat flow model for friction stir welding of aluminum alloys", J. Mater. Process. Manuf. Sci. 7, pp. 185–194.

Lin, C.Y. and Hajela, P., 1992, "Genetic algorithms in optimization problems with discrete and integer design variables", Engineering Optimization. Vol. 19, pp. 309-327.

Midling O.T., 1999, "Effect of tool shoulder material on heat input during friction stir welding", Proceedings of the First International Symposium on Friction Stir Welding, Thousands Oaks, CA, USA, pp. 14-16.

Sousa, F.L., Ramos, F.M., Paglione, P., and Girardi, R. M., 2003, "New Stochastic Algorithm for Design Optimization", AAIA Journal, Vol. 41., No. 9., pp. 1808-1818.

Reynolds A.P., Lockwood W.D., and Seidel T. U., 2000, "Processing–property correlation in friction stir welds", Mater. Sci. Forum, pp. 1719-1724.

Russell M.J. and Sheercliff H.R., 1999, "Analytic modeling of microstructure development in friction stir welding", Proceedings of the First International Symposium on Friction Stir Welding, Thousands Oaks, CA, USA, pp. 14-16.

Talwar R., Bolser B., Lederich R., and Baumann J., 2000, "Friction stir welding of airframe structures", Proceedings of the Second International Symposium on Friction Stir Welding, Gothenburg, Sweden, pp. 26-28.

Tang W., Guo X., McClure J.C., Murr L.E., and Nunes A., 1998, "Heat input and temperature distribution in friction stir welding", J. Mater. Process. Manuf. Sci. 7, pp. 163-172.

Zhu X.K., and Chao Y. J., 2004, "Numerical simulation of transient temperature and residual stresses in friction stir welding of 304L stainless steel", Journal of Materials Processing Technology 146, pp. 263-272.

10. RESPONSIBILITY NOTICE

The authors are the only responsible for the printed material included in this paper.